This article has been accepted for publication in a future issue of this journal, but has not been fully edited. Content may change prior to final publication. Citation information: DOI 10.1109/JBHI.2015.2417805, IEEE Journal of Biomedical and Health Informatics

# In-Body to On-Body Ultra Wideband Propagation Model Derived from Measurements in Living Animals

Pål Anders Floor, Raúl Chávez-Santiago, Sverre Brovoll, *Member, IEEE*, Øyvind Aardal, Jacob Bergsland, Ole-Johannes H. N. Grymyr, Per Steinar Halvorsen, Rafael Palomar, Dirk Plettemeier, Svein-Erik Hamran, Tor A. Ramstad, and Ilangko Balasingham, *Senior Member, IEEE*

***Abstract*—Ultra wideband (UWB) radio technology for wireless implants has gained significant attention. UWB enables the fabrication of faster and smaller transceivers with ultra low power consumption, which may be integrated into more sophisticated implantable biomedical sensors and actuators. Nevertheless, the large path loss suffered by UWB signals propagating through inhomogeneous layers of biological tissues is a major hindering factor. For the optimal design of implantable transceivers, the accurate characterization of the UWB radio propagation in living biological tissues is indispensable. Channel measurements in phantoms and numerical simulations with digital anatomical models provide good initial insight into the expected path loss in complex propagation media like the human body, but they often fail to capture the effects of blood circulation, respiration, and temperature gradients of a living subject. Therefore, we performed UWB channel measurements within 1-6 GHz on two living porcine subjects because of the anatomical resemblance with an average human torso. We present for the first time a path loss model derived from these in-vivo measurements, which includes the frequency-dependent attenuation. The use of multiple on-body receiving antennas to combat the high propagation losses in implant radio channels was also investigated.**

***Index Terms*—channel model, implant, in-body, in-vivo, path loss**

This work is part of the MELODY Project-Phase II (Contract no. 225885), which is financially sponsored by the Research Council of Norway.

P.-A. Floor, R. Chávez-Santiago, J. Bergsland, O.-L. H. N. Grymyr, P. S. Halvorsen and I. Balasingham are with the Intervention Centre, Oslo University Hospital, NO-0027 Oslo, Norway (e-mail: andflo@rr-research.no; raul.chavez-santiago@rr-research.no; jacobbergsland622@ googlemail.com; olegry@ous-hf.no; sthalvor@ous-hf.no; ilangko.balasingham@ medisin.uio.no). They all are also with the Institute of Clinical Medicine, University of Oslo. P.-A. Floor, R. Chávez-Santiago and I. Balasingham are also with the Norwegian University of Science and Technology (NTNU).

S. Brovoll, Ø. Aardal and S.-E. Hamran are with the Norwegian Defence Research Establishment (FFI), NO-2027 Kjeller, Norway (e-mail: Sverre.Brovoll@ffi.no; Oyvind.Aardal@ffi.no; Svein-Erik.Hamran@ffi.no).

R. Palomar is with The Norwegian Colour and Visual Computing Laboratotory, Gjøvik University College, NO-2815 Gjøvik, Norway (e-mail: Rafael.Palomar@rr-research.no). He is also with the Intervention Centre, Oslo University Hospital.

D. Plettemeier is with the Dresden University of Technology, D-01069 Dresden, Germany (dirk.plettemeier@tu-dresden.de).

T. A. Ramstad is with the Norwegian University of Science and Technology (NTNU), NO-7491 Trondheim, Norway (e-mail: ramstad@iet.ntnu.no).

## I. Introduction

DATA from the World Health Organization (WHO) indicate that the global population suffering from chronic diseases is increasing at an alarming rate. It has been estimated that in 2001 chronic diseases contributed to approximately 60% of the reported deaths worldwide. It is forecasted that by 2020 nearly three-quarters of deaths in the world will be caused by chronic conditions like diabetes and ischemic heart disease (IHD) [1]. For the prevention and better management of chronic diseases the involvement of the patients themselves is crucial. This can be achieved with the real-time monitoring of various physiological signals. The use of telecommunications and microelectronic technology can significantly contribute to this goal through the development of radio frequency (RF) wireless biomedical sensors [2]. For instance, continuous glucose monitoring (CGM) systems [3] utilizing subcutaneous RF implantable sensors can contribute greatly to the self-management of diabetes. Other in-body sensors like the wireless capsule endoscope (WCE) [4]-[6] facilitate the diagnosis of disease in the small bowel, which is difficult to visualize with conventional endoscopic techniques.

The IEEE Standard 802.15.6™-2012 specifies the physical (PHY) and medium access control (MAC) layers for communication between small RF transceivers deployed on the surface, inside, or in the peripheral proximity of the human body [7]. Combined with various biomedical sensors, real-time measurement and monitoring of physiological signals becomes possible with this technology. The centrally-coordinated or distributed interconnection of wireless biomedical sensors, referred to as a body area network (BAN), can be implemented in existing industrial, scientific, medical (ISM) bands as well as other portions of the electromagnetic spectrum approved by national medical and/or regulatory authorities. Although IEEE Standard 802.15.6 ™-2012 does not consider the use of ultra wideband (UWB) signals for in-body biomedical devices, the feasibility of high data rate communication for implantable devices using UWB signals has been demonstrated in a number of studies [8]. As defined by the United States Federal Communications Commission (FCC), UWB signals are those with fractional bandwidth exceeding 20% of the center frequency, or alternatively, a

This article has been accepted for publication in a future issue of this journal, but has not been fully edited. Content may change prior to final publication. Citation information: DOI 10.1109/JBHI.2015.2417805, IEEE Journal of Biomedical and Health Informatics

bandwidth greater than 500 MHz. UWB communication systems have the ability to operate with ultra lower power and low signal-to-noise ratio (SNR) using different modulation and coding strategies, characteristics that are attractive for the wireless interfaces of implantable biomedical sensors. Additionally, UWB signals may not represent a threat to patients' safety [9]. In the United States UWB outdoor/indoor communication systems are allowed to operate within 3.1-10.6 GHz according to FCC spectrum regulations, whereas in other parts of the world different sub-bands within this spectrum portion are used according to local regulations.

Computer simulations of in-body to on-body (IB2OB) communications, i.e., a wireless link between a sensor operating inside the human body and an on-body gateway device, have suggested that data rates as high as 100 Mbit/s are feasible using UWB [10], [11]. Nevertheless, an in-vivo experiment on a living porcine subject demonstrated a significantly lower data rate of 1 Mbit/s and a bit error rate (BER) of $10^{-2}$ for an UWB link between a transmitter implanted at a maximal depth of 12 cm into the abdominal cavity and an on-body receiver [12]. This discrepancy calls for further research to determine whether a sensor implanted into the human body at a depth of several centimeters could actually communicate at data rates in the order of tens of Mbits/s using an UWB interface. The large path loss suffered by UWB signals propagating through living biological tissues is the main hindering factor. Therefore, accurate characterization of the radio channel is necessary to enhance the design and optimization of implantable RF transceivers.

Nevertheless, there have been limited attempts to model the IB2OB channel for UWB implants. To the best of our knowledge, the first IB2OB UWB channel model was reported in [13], which stemmed from numerical simulations using a voxel anatomical model. To collect channel data an implantable disc dipole antenna was designed, which covered the frequency band of 3.4-4.8 GHz. Although the channel impulse response (CIR) for propagation in the thoracic cavity was obtained, no path loss formulas were presented therein. A more elaborated model providing a statistical description of both the CIR and path loss of an IB2OB UWB link within 1-6 GHz for the thoracic cavity was presented in [14]. This model was derived from numerical simulations using the voxel anatomical data set of the Visible Human Project®. In addition to path loss, the model predicted a root-mean square (RMS) delay spread below 1 ns. Further improvement by including the frequency-dependent attenuation was introduced to this model in [15].

Despite the reliability of modern anatomical voxel models and electromagnetic simulation tools, the best way of gathering accurate channel data for an IB2OB propagation model consists of performing measurements in a realistic propagation medium, i.e., living biological tissues. This facilitates capturing the effects of blood circulation, respiration, and temperature gradients of a living subject. Therefore, expansion of research to involve expertise from the healthcare domain to develop more accurate propagation models for implant communications was devised in [16] as an important strategy. Nevertheless, for practical and ethical reasons such measurement campaigns with humans are not possible. Therefore, performing channel measurements in living animals that anatomically resemble parts of the human body is a viable alternative.

In the following we present a path loss model for the IB2OB UWB channel derived from in-vivo measurements on two living porcine subjects. To the best of our knowledge, this is the first IB2OB UWB path loss model derived from in-vivo measurements that is reported in the literature. Scattering matrices were measured at different implantation depths in the abdominal cavity using a single implanted UWB antenna and one or two on-body antennas. From these matrices we obtained measurements of the forward channel gain in the frequency domain, i.e., the $S_{21}(f)$ parameter, at different implantation depths, which were later processed in Matlab™ to derive the path loss of each link as $-PL = \text{mean}\{|S_{21}(f)|\}$ in decibels (dB). The proposed path model describes average behavior of all the channel measurements obtained within 1-6 GHz and is valid for implantation depths ranging 5-16 cm. An investigation of simultaneous reception with two antennas was also undertaken in order to assess the possible use of multiple antennas to recover more of the power transmitted from inside the body. The use of multiple receiving antennas may help to tackle the effects of the very large path loss typically observed in IB2OB channels [17].

The remainder of the paper is organized as follows: In Section II, the experimental methodology is described in detail and some channel measurements are presented. In Section III the IB2OB path loss model is derived based on the obtained measurements. In Section IV we investigate the use of multiple on-body receiving antennas. Finally, in Section V, our conclusions are given and future work is briefly discussed.

## II. Experimental Setup and Methodology

The measurement campaigns were undertaken at the Intervention Centre, Oslo University Hospital, with the approval of the Norwegian Animal Research Authority (NARA). Because of the appropriate size to approximate the anatomy of an average human torso, two Norwegian landrace female pigs with body weights of 42 kg and 46 kg, respectively, were utilized in two separate experiments. During both procedures, humane treatment was provided to the experimental subjects by researchers certified with FELASA[1] Category C (European Convention for the Protection of Vertebrate Animals (ETS No. 123)) in accordance to standard clinical protocol. Laparotomy was performed in order to enable the implantation of an in-body (IB) probing antenna at various depths in the abdominal cavity. The measurement points where the on-body (OB)

[1] FELASA stands for Federation of European Laboratory Animal Science Associations, which has established an accreditation system for teaching programs for all categories of personnel involved in the care and use of laboratory animals. The FELASA Accreditation Scheme is intended for courses that educate and train persons for Functions A, B, C & D defined in article 23 of EU Directive 2010/63.

This article has been accepted for publication in a future issue of this journal, but has not been fully edited. Content may change prior to final publication. Citation information: DOI 10.1109/JBHI.2015.2417805, IEEE Journal of Biomedical and Health Informatics

receiving antenna(s) were placed on the anesthetized porcine subject during the first experiment are indicated in Fig. 1 whereas the swine anatomy is depicted in Fig. 2 [18]. A small surgical incision in each case was made on the side of the animal to insert the IB antenna. In order to avoid coupling between the IB and OB antennas through creeping waves, the point of entry was carefully covered with electromagnetic insulating material.

An electromagnetic tracking system (NDI Aurora®) measured the distance between the IB and OB antennas with an RMS error margin of 0.7 mm. The IB and OB antennas were connected to the ports of a Rohde & Schwarz™ ZVA67 vector network analyzer (VNA) through shielded coaxial cables of 2 meters in length. The cables' frequency response was subtracted from the channel measurements by performing a full-calibration of the VNA. Electromagnetic compatibility (EMC) tests were performed in order to ensure that unwanted electromagnetic emissions from collocated electronic devices like the electromagnetic tracking system did not interfere with the UWB communication system.

The scatter matrix was obtained for all the points indicated in Fig. 1 during the first experiment as well as 16 additional points (in the same area as in Fig. 1) during the second experiment.

### *A. In-Body (IB) Probing Antenna*

Because of the difficulty to keep the IB and OB antennas aligned with respect to each other during the in-vivo measurements, an UWB implantable antenna with quasi-omnidirectional radiation pattern had to be employed. This consideration corresponds to some practical in-body medical sensor applications like the WCE, in which quasi-omnidirectional antennas are used to establish the IB2OB radio communication link because of the unpredictable orientation that the device can have as it travels inside the gastrointestinal (GI) tract [4]-[6].

Hence, for the IB probing antenna a conformal trapezoid strip excited broadband hemispherical dielectric resonator antenna (DRA) [19] was utilized. This implantable DRA was originally designed for optimal operation within 3.1-4.8 GHz for possible application in WCEs. With a diameter of just 8 mm (Fig. 3), this antenna design facilitates the implantation while providing the adequate radiation pattern for the measurements. The DRA was implanted into the abdominal cavity in the area of the small intestine within the area delimited by the green border indicated in Fig. 2.

During the first experiment the DRA was implanted at two different depths, 5 cm and 9 cm, measured from the reference points 1 (P1) and 8 (P8) in Fig. 1, respectively. Table I shows the distance between each measurement point in Fig. 1 and the IB probing antenna. Note that for an implantation depth of 9 cm only P8, P9, and P10 were considered.

In the second experiment the DRA was implanted at depths of 6 cm, 7 cm, and 13 cm. Table II shows the distance between each of the measurement points (here labeled as E2 for "Experiment 2") and the IB probing antenna. Points P1E2, P10E2 and P18E2 are reference points for the implantation depths of 6 cm, 7 cm, and 13 cm, respectively.

In both experiments, and for each point, the measurements were repeated 8-12 times over 4-5 minutes in order to reveal and account for any significant change in the propagation medium over time.

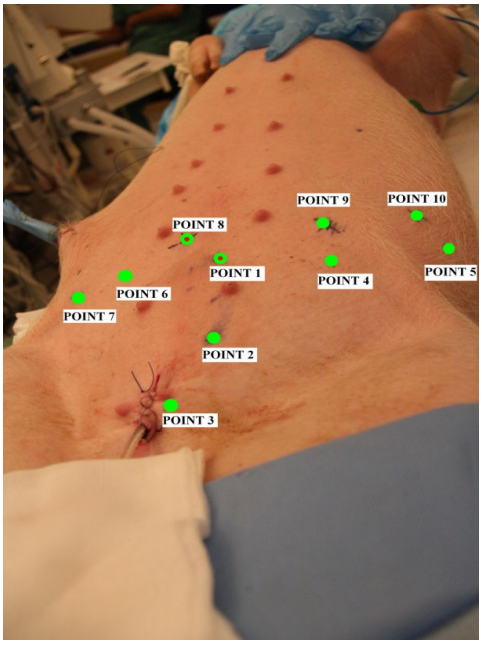


Fig. 1. Measurements points on the anesthetized swine for the first experiment.

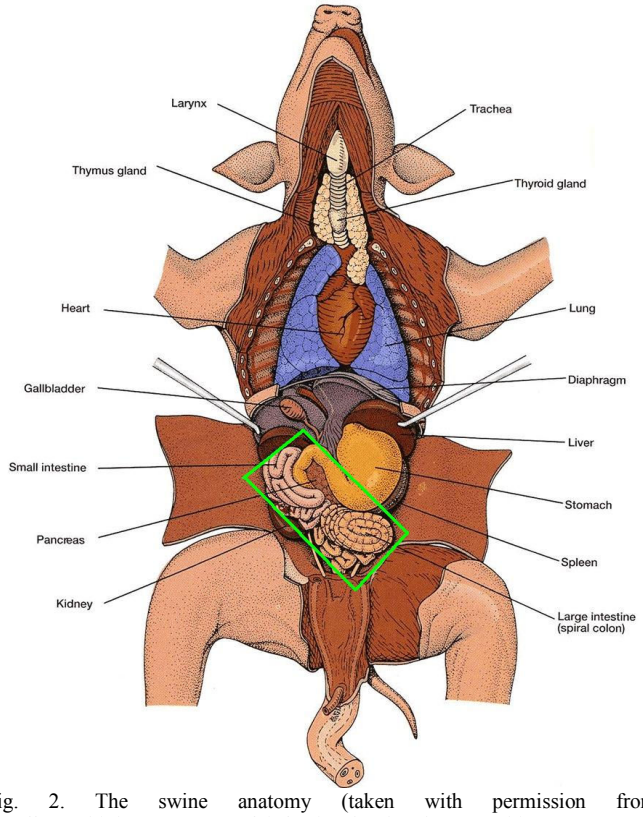


Fig. 2. The swine anatomy (taken with permission from http://www.biologycorner.com/pig/review.html). The IB probing antenna was implanted within the area delimited by the green border.

This article has been accepted for publication in a future issue of this journal, but has not been fully edited. Content may change prior to final publication. Citation information: DOI 10.1109/JBHI.2015.2417805, IEEE Journal of Biomedical and Health Informatics

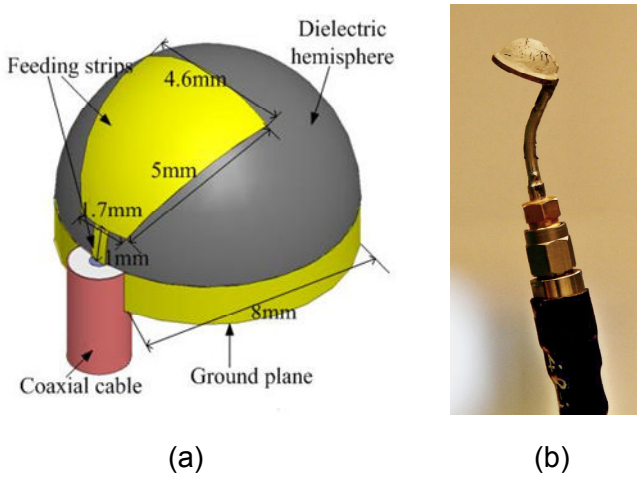


Fig. 3. (a) Dimensions and (b) physical implementation of the UWB IB antenna. The radiation pattern and technical details of this antenna can be found in [19].

TABLE I
DISTANCES BETWEEN IB AND OB ANTENNAS IN EXPERIMENT 1

| Point | Distance from IB antenna implanted at 5 cm depth | Distance from IB antenna implanted at 9 cm depth |
|---|---|---|
| P1 | 5 cm | × |
| P2 | 10 cm | × |
| P3 | 15 cm | × |
| P4 | 10 cm | × |
| P5 | 15 cm | × |
| P6 | 6.5 cm | × |
| P7 | 10 cm | × |
| P8 | × | 9 cm |
| P9 | × | 13 cm |
| P10 | × | 16 cm |

TABLE II
DISTANCES BETWEEN IB AND OB ANTENNAS IN EXPERIMENT 2

| Point | Dist. from IB antenna implanted at 7 cm depth | Dist. from IB antenna implanted at 6 cm depth | Dist. from IB antenna implanted at 13 cm depth |
|---|---|---|---|
| P1E2 | 7 cm | × | × |
| P2E2 | 12 cm | × | × |
| P3E2 | 9 cm | × | × |
| P4E2 | 12 cm | × | × |
| P5E2 | 7.5 cm | × | × |
| P6E2 | 10 cm | × | × |
| P7E2 | 7 cm | × | × |
| P8E2 | 8.5 cm | × | × |
| P9E2 | × | 6 cm | × |
| P10E2 | × | 8 cm | × |
| P11E2 | × | 7.5 cm | × |
| P12E2 | × | 7 cm | × |
| P13E2 | × | 7 cm | × |
| P14E2 | × | 8 cm | × |
| P15E2 | × | × | 13 cm |
| P16E2 | × | × | 14 cm |

### B. *On-Body (OB) Receiving Antenna*

The OB receiving antenna was an UWB bowtie dipole [20] made of conductive patches on a printed-circuit board (PCB) with a total size of 3.6×7.6 cm$^2$ (Fig. 4). As in the case of the IB probing antenna, the bow tie dipole exhibited a quasi-omnidirectional radiation pattern.

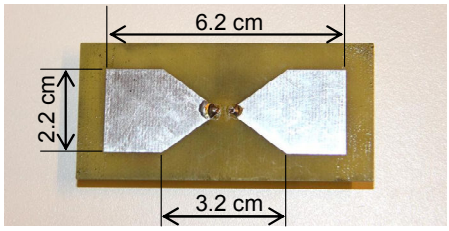


Fig. 4. Physical implementation and dimensions of the UWB OB antenna.

In the first experiment, measurements with a single bowtie dipole were taken at P1, P2, P3, and P8. Furthermore, in order to investigate whether several antennas could be used for reception as well as determining the correlation between different propagation paths, two OB antennas were placed 8 cm from each other to simultaneously obtain measurements at P4, P5, P6, P7 (with one of the bowtie dipoles fixed at P1) as well as P9 and P10 (with a bowtie dipole fixed at P8). In the second experiment, the OB receiving antennas were placed even closer to each other (between 3-5 cm), and during some of these measurements a smaller bowtie dipole antenna [20] of total size 2.5×5 cm$^2$ had to be applied (see Section IV).

### C. *Reflection Coefficient of the IB Antenna*

For implantation the IB probing antenna had to be covered with a thin layer of nitrile butadiene rubber (NBR), which is a polymer commonly used for the fabrication of disposable laboratory gloves. The cover was applied manually by wrapping the antenna in a pre-fabricated thin sheet of NBR, which was sealed tightly with tape after extracting the air between the antenna's surface and the polymer. This was done to prevent physical contact with the abdominal fluids, which could have short-circuited the printed board elements or the connector thereby rendering the antenna inoperative. Through measurements of the $S_{11}$ parameter in a tissue-simulating phantom solution [21] with and without the NBR protective layer, we concluded that the presence of this thin layer of polymer did not change significantly the radiating characteristics of the antenna. When implanted in the swine's abdominal cavity, however, the $S_{11}$ parameter of the IB probing antenna (Fig. 5(a)) differed significantly from the $S_{11}$ obtained through numerical simulations and measurements in a tissue-simulating liquid phantom [19]. Reportedly, the $S_{11}$ parameter in a phantom had a value of −10 dB within 3-5 GHz. This significant discrepancy with our results reinforces the claim that in-vivo measurements are necessary in order to include some effects that are not captured by simulations or measurements in homogeneous propagation media like phantoms. Disregarding such effects may lead to over-

This article has been accepted for publication in a future issue of this journal, but has not been fully edited. Content may change prior to final publication. Citation information: DOI 10.1109/JBHI.2015.2417805, IEEE Journal of Biomedical and Health Informatics

optimistic estimation of the antenna characteristics and propagation conditions.

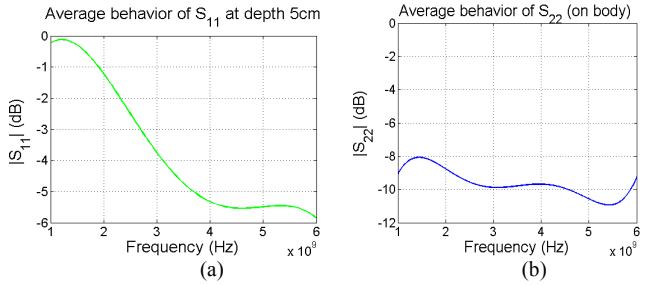


Fig. 5. (a) Reflection coefficient of the IB probing and (b) OB receiving antennas, averaged over 30 measurements for an implantation depth of 5 cm.

Although the reflection coefficient of the IB probing antenna was rather high for frequencies below 3 GHz as seen in Fig. 5(a), it is possible to compensate for the antenna response by using the $S_{11}$ parameter averaged over many measurement repetitions. Since the channel attenuation is very high, which implies a high isolation between the IB and OB antennas, and considering that the $S_{22}$ exhibits good behavior within 1-6 GHz (see Fig. 5(b)), the compensation can be done by considering $S_{11}$ only. Since the $S_{11}$ parameter acts as the reflection coefficient whenever all the other VNA ports (here Ports 2 and 3) are well-matched, the power that is coupled into the swine's body is given by

$$\widetilde{P}_{\mathrm{Tx}} = P_{\mathrm{Tx}}\left(1-\left|S_{11}\right|^2\right), \tag{1}$$

where $P_{\mathrm{TX}}$ is the power delivered at Port 1 of the VNA. However, when the VNA computes the $S_{21}$, it considers the ratio between a wave coming out of Port 2 and a wave going into Port 1, given that Port 2 is matched impedance-wise (i.e., there is no wave reflected into Port 2). This implies that the output/input power ratio based on the VNA measurements are given by $\left|S_{21}\right|^2 = P_{\mathrm{RX}}/P_{\mathrm{TX}}$. However, since only the power $\widetilde{P}_{\mathrm{Tx}}$ is coupled into the animal's body, a more realistic value of $\left|S_{21}\right|^2$ is obtained by the ratio

$$\left|\widetilde{S}_{21}\right|^2 = \frac{P_{\mathrm{RX}}}{P_{\mathrm{TX}}} = \frac{P_{\mathrm{TX}}\left|S_{21}\right|^2}{P_{\mathrm{TX}}\left(1-\left|S_{11}\right|^2\right)} = \frac{\left|S_{21}\right|^2}{1-\left|S_{11}\right|^2}. \tag{2}$$

This value will be substantially different from $\left|S_{21}\right|^2$ when $\left|S_{11}\right|$ is close to unity. In the remainder of this paper both compensated and non-compensated forward transmission coefficients will be evaluated, i.e., $\left|\widetilde{S}_{21}\right|^2$ and $\left|S_{21}\right|^2$, respectively. The non-compensated data will serve as a pessimistic estimate of the path loss, whereas the compensated data will be closer to what can be expected in practical propagation situations. As an example, Fig. 6 shows the channel forward transmission coefficient (gain) for a single measurement trial compared to the average over 10 trials for P1 and P8. From these figures one can observe that the channel gain does not change abruptly over the course of several minutes within 1-6 GHz for P1 and 1-3 GHz for P8.

Figure 7 shows the compensated and non-compensated channel gain measurements for P1 and P8. Notice that 10-15 dB reduction in the attenuation is observed at 1 GHz when the measured gain is compensated, which is more in agreement with simulation results [11].

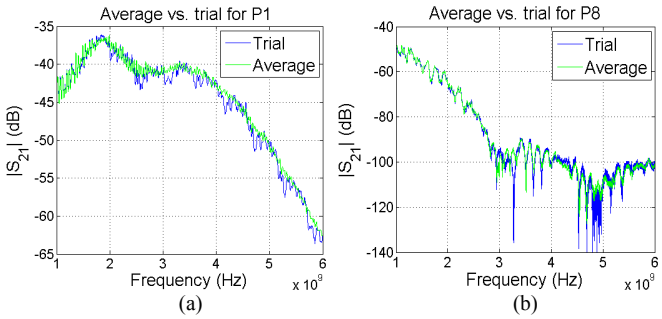


Fig. 6. Average versus one-trial channel gain measurements for (a) P1 and (b) P8.

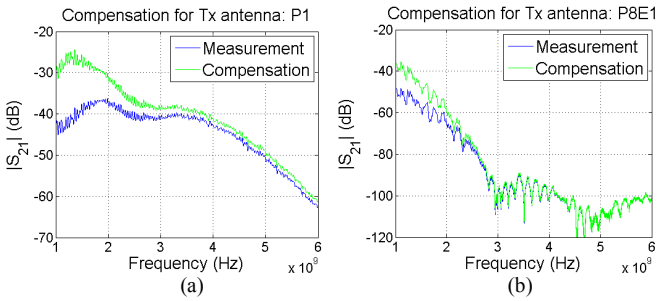


Fig. 7. Compensated versus non-compensated channel gain measurements for (a) P1 and (b) P8.

## III. Path Loss Model

A path loss formula as a function of the propagation distance was obtained by fitting exponential curves to the data obtained from all the $S_{21}$ measurements in all the points listed in Tables I and II. The well-known log-distance model for in-body channels given in [22] was applied as

$$PL(d) = PL_0 + 10n\log_{10}\left(\frac{d}{d_0}\right), \tag{3}$$

where $d$ is the separation between antennas, i.e., implantation depth in centimeters, and $d_0$ is the reference implantation depth with a value of 5 cm, i.e., the minimal depth for which we were able to obtain measurements. $PL_0$ is the path loss at the reference depth $d_0 = 5$ cm and was obtained from the measurements at P1. The path loss exponent $n$ was found by a non-linear least squares curve fitting algorithm. Figure 8 shows both the scatter plot for all the obtained measurements as well as the curve fitting for 1 GHz and 4 GHz, respectively.

Because of the frequency-dependency of the dielectric constants of the different organs and tissues along the propagation path [15], the rate at which the path loss increases with distance is a function of frequency, $f$. This rate is expressed by the path loss exponent, which as a function of

This article has been accepted for publication in a future issue of this journal, but has not been fully edited. Content may change prior to final publication. Citation information: DOI 10.1109/JBHI.2015.2417805, IEEE Journal of Biomedical and Health Informatics

frequency is denoted as $N(f)$. This parameter closely follows a 2nd degree polynomial of the form

$$N(f) = af^2 + bf + c \quad (4)$$

where $a$, $b$, and $c$ are fitting coefficients, the optimal values of which are given in Table III. Figure 9 shows how the path loss exponent model in (4) approximates the channel measurements within the entire frequency band of 1-6 GHz. Note that these coefficients may change if the reference depth $d_0$ changes too. Hence, the presented model is valid for $5 \le d \le 16$ cm only.

By inserting (4) into (3) and using the data obtained from P1 to determine $PL_0$, the two-dimensional path loss profiles in Fig. 10 as a function of both frequency and depth were obtained. From these graphics it is clear that the propagation in lower frequencies (approximately within 1-3 GHz) exhibit significantly lower path loss. Moreover, the rate at which the path loss increases with depth is much higher as frequency increases. Also notice that the rate at which the path loss increases with frequency is larger as depth grows. To illustrate the last statement we have compared three path loss curves as a function of frequency for three different depths in Fig. 11. We set all the curves to the starting point of 0 dB to observe the relative path loss with respect to each other, i.e., the different rates of path loss change. Evidently, the rate at which path loss increases as a function of frequency becomes more severe at higher depths. This can be explained by the inhomogeneity of organs and tissues in the deep abdominal cavity, contrasting the lower depths in which more homogeneous layers of skin, fat, and muscle tissues are found.

The propagation effects described above were also observed in [15] from numerical simulations. The characterization of all these path loss variations over depth and frequency provides useful guidelines for the design of wireless implant communications. Due to the lower path losses in lower frequencies, the power consumption of implantable UWB transceivers could be reduced even further by transmitting within 1-3 GHz. This would increase the operational life span of UWB biomedical implants. As mentioned in the Section I, spectrum regulations constrain the utilization of UWB to 3.1-10.6 GHz for indoor and outdoor propagation environments. Nevertheless, regulating the use of 1-3 GHz for in-body UWB transmissions [23] would be highly beneficial for the use of this RF technology in applications that demand high data transmission rates like the WCE [4]-[6].

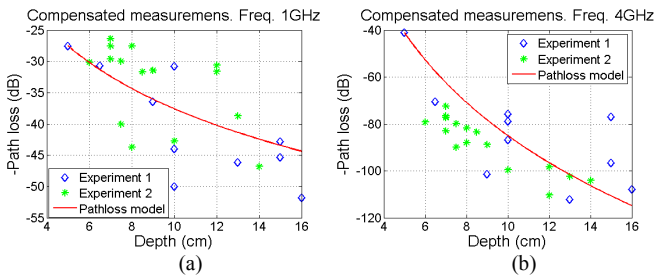


Fig. 8. Curve fitting to path loss measurements at (a) 1 GHz and (b) 4 GHz.

TABLE III
COEFFICIENTS FOR QUADRATIC FITTING TO PATH LOSS EXPONENT

| | *a* | *b* | *c* |
|---|---|---|---|
| No compensation | –0.813 | 7.817 | –3.235 |
| Compensation | –0.800 | 7.839 | –3.647 |

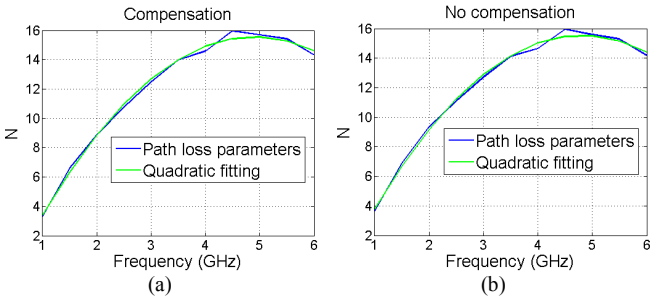


Fig. 9. Path loss exponent fitting for the (a) non-compensated and (b) compensated data.

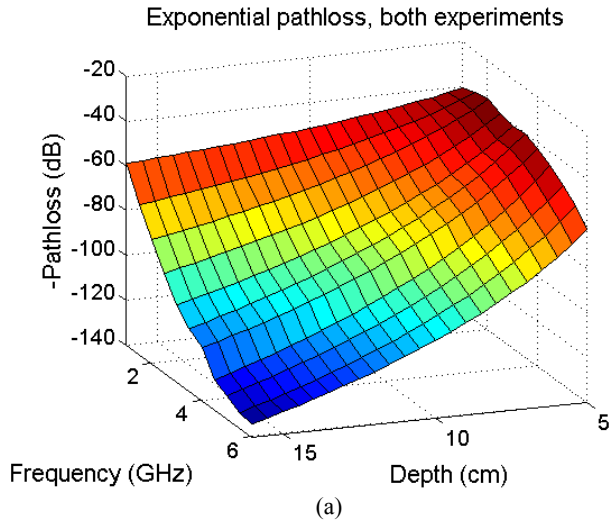


Fig. 10. Path loss as a function of frequency and implantation depth for (a) non-compensated and (b) compensated measurements.

This article has been accepted for publication in a future issue of this journal, but has not been fully edited. Content may change prior to final publication. Citation information: DOI 10.1109/JBHI.2015.2417805, IEEE Journal of Biomedical and Health Informatics

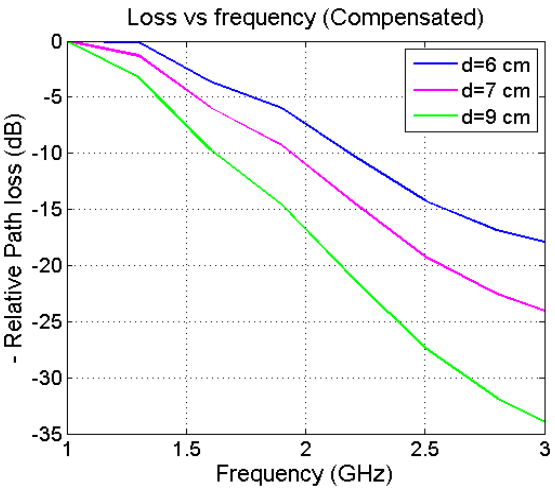


Fig. 11. Path loss slopes over frequency for different depths within 1-3 GHz.

## IV. Multiple Receiver Antennas

One way of extracting more of the power transmitted from the quasi-omnidirectional IB antenna is to use multiple OB receiving antennas placed at different points on the porcine subject's abdomen [17]. This can reduce some of the large losses observed in Fig. 10, given that the reception from each antenna is strong enough. In the following, the gains from multiple antennas as well as the correlations between different propagation paths are investigated.

### A. Gain from Multiple Antennas

In order to investigate the use of multiple antennas, two OB receiving antennas were applied simultaneously on the skin of the porcine subject and 3×3 measurement scatter matrices were obtained with the VNA. Simultaneous measurements were done between points P1 and P4-P7, P8 and P9-P10 (see Table I), P1E2 and P3E2-P8E2, P9E2 and P10E2-P14E2, as well as P15E2 and P16E2 (see Table II). Three different distances separating the two OB receiving antennas were considered: 8 cm (e.g., between P1 and P6), 5 cm (e.g., between P1E2 and P6E2) and 3 cm (e.g., between P9E2 and P12E2).

In order to place the antennas as close as 3 cm from each other, the smaller bowtie antenna design described in Subsection II.A had to be used; the smaller bowtie antennas exhibited an $S_{22}$ behavior similar to the bigger-size one's. When placing the antennas as close as 3-5 cm from each other it is also important to investigate their mutual coupling. The coupling can be observed from the $S_{32}$ parameter averaged over 8 measurement trials and plotted in Fig. 12. As seen, the mutual coupling is highest at 1 GHz when the antennas are at 3 cm distance, but it falls off rapidly as the frequency increases. We concluded that this mutual coupling was acceptably low.

Here, we tried to obtain insight into the typical gains that may be achieved with the use of multiple antennas. We therefore considered a rather ideal scenario where the channel can be perfectly estimated at the receiver. We chose to cover the frequency band of 1-4 GHz by using a Gaussian window

$$H_G(f)=\begin{cases} e^{\frac{f-\mu}{2\sigma^2}}, f\in[f_l,f_u] \\ 0 \quad\quad , f\in[f_l,f_u] \end{cases}, \tag{5}$$

where $f_l=1$ GHz and $f_u=4$ GHz. With $\mu=2.5$ GHz and $\sigma=0.68$, the −3 dB points occur at 2 GHz and 3 GHz, respectively. The total response is then $H_{\mathrm{Rx1}}=H_G(f)S_{21}(f)$ between the input and output of Antenna 1 and $H_{\mathrm{Rx2}}=H_G(f)S_{31}(f)$ between the input and output of Antenna 2. Both $S_{21}$ and $S_{31}$ were obtained by averaging measurements for the relevant points over 8-10 trials. At the receiver, a filter matched to the whole response, $H_{\mathrm{Rx1}}$, was applied:

$$H_{\mathrm{MF}_i}=\kappa\cdot H^*_{\mathrm{Rx}_i}(f)\cdot e^{-j2\pi fT_i}, \tag{6}$$

In (6), the exponential is a phase term depending of the delay of path $i$, $T_i$, and $\kappa$ is a constant, one specific example of which is given in [24]. This filter maximizes the peak signal-to-noise ratio (SNR) at the receiver $i$, which is given by

$$\gamma_i=\frac{1}{N_0}\int_{f_l}^{f_u}\left|H_{\mathrm{Rx}i}(f)\right|^2 df=\frac{1}{N_0}\alpha_i, \tag{7}$$

where $N_0$ is the noise power spectral density (PSD). This is a well-known result in communication theory. For further details the reader may consult [25, pp.414-415]. With $\gamma_1\geq\gamma_2$, the SNR gain from two antennas can be computed as

$$G=10\log_{10}\left(\frac{\gamma_1+\gamma_2}{\gamma_1}\right)=10\log_{10}\left(\frac{\alpha_1+\alpha_2}{\alpha_1}\right). \tag{8}$$

The last equality is due to the noise PSD cancelling out. Figure 13 shows the channel impulse response (CIR) for P9E2 (green) and P12E2 (red). The distance between these two points was 3 cm and the CIR was obtained by performing the IFFT of $H_{\mathrm{Rx}_j}(f)$. For these two points, one can calculate a gain of $G=2.1$ dB. Note that the highest possible gain using two antennas simultaneously is 3 dB, which is obtained when $\alpha_1=\alpha_2$. Table IV summarizes the gain obtained at some selected points (P$i$P$j$E2 denotes point $i$ and point $j$ from Experiment 2, respectively).

From these results several interesting features can be noticed. First of all, it is convenient to use multiple antennas since a significant power gain can be achieved. Take P1E2; with one antenna placed at 3 cm distance (at P8E2) and one at 5 cm distance (at P5E2) one can gain approximately 3.2 dB, which is equivalent to doubling the received power. With more antennas at both sides of P1E2 (and any reference point in general), the gain may be even higher. However, as Table IV shows, there are large variations in the gain that can be obtained. Now take P1P5E2 and P1P6E2 where 1.28 dB and 0.22 dB are gained, respectively. Although these two gains are obtained for the same antenna distance, their difference in dB is significant. There are three main reasons for this phenomenon:

1) Since the experimental subject's surface is not flat, the IB to OB distance from the second antenna may vary. For

This article has been accepted for publication in a future issue of this journal, but has not been fully edited. Content may change prior to final publication. Citation information: DOI 10.1109/JBHI.2015.2417805, IEEE Journal of Biomedical and Health Informatics

example, P5E2 is 7.5 cm from the IB probing antenna whereas P6E2 is 10 cm away, as seen in Table II.

2) The dielectric properties can differ from point to point because of different types of biological tissues along each propagation path. This implies that the gain may be different even if the distances between OB antennas as well as the distances between IB to OB antennas are the same.

3) The IB antenna's radiation pattern is not isotropic.

Hence, in practice one way of implementing an on-body receiver for IB2OB UWB communication links can be the use of a belt around the waist with many antennas embedded in it. In order to pick out the antennas with the best gain at any time, it is important to implement a selection algorithm at the receiver. If the implant sends pilot signals at certain fixed time intervals, the algorithm can select the subset of antennas with the best reception at any given time. The design of such on-body receiver opens many opportunities for research in signal processing for wireless implants.

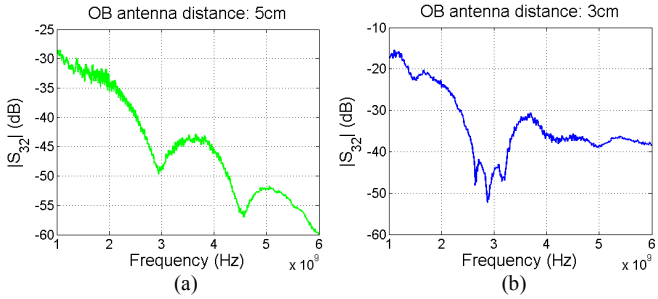


Fig. 12. Example of mutual coupling between two OB receiving antennas at (a) 5 cm and (b) 3 cm from each other.

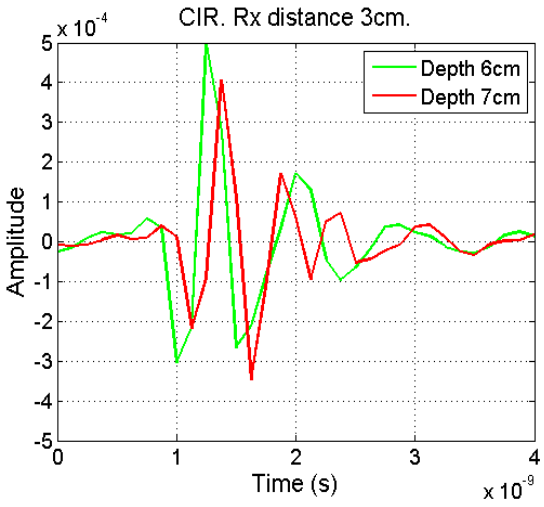


Fig. 13. CIR obtained in P9E2 and P12E2.

TABLE IV
GAIN FOR DIFFERENT ON-BODY RECEIVING ANTENNA DISTANCES

| Distance: 8 cm | Distance: 5 cm | Distance: 3 cm |
|---|---|---|
| 0.18 dB (P1P6) | 1.23 dB (P1P5E2) | 2.09 dB (P9P12E2) |
| 0.16 dB (P1P4E2) | 0.22 dB (P1P6E2) | 1.1 dB (P1P7E2) |
| 0.34 dB (P8P9) | 1.67 dB (P15P16E2) | 1.98 dB (P1P8E2) |

### B. *Inter-Channel Correlations*

When constructing signal processing and communication algorithms for multiple receivers (e.g., for applications like combining, localization and tracking of moving devices, etc.), it is important to know the correlation between the different propagation paths.

In order to determine the correlation between different paths in our measurements, the cross-correlation function (CCF) was calculated between the CIRs obtained through simultaneous measurements at several points. The same band and window as in Subsection IV.A were assumed. The CCF computed was normalized so that the (auto)-correlation between two equal signals would be 1 at lag 0. Figure 14 shows the correlation between some selected points from Tables I and II for distances separating the OB receiving antennas of 3 cm, 5 cm, and 8 cm, respectively.

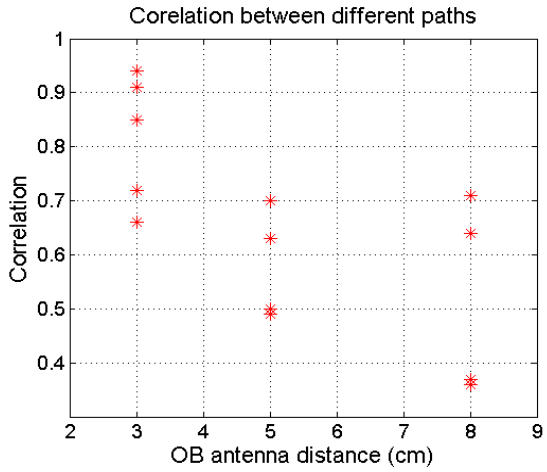


Fig. 14. Maximal correlation between CIRs from two propagation paths at different distances.

Although the spreads of the correlation values are significant for a given antenna separation, the clear trend is that the correlation increases as the distance between antennas decreases. The correlation is generally quite high, which is expected since the different paths do not change significantly over the course of several minutes. Note that a high power gain between two OB receiving antennas does not necessarily imply a higher correlation value. For example, the correlation between P1E2 and P7E2 is 0.91 with a gain of 1.1 dB, whereas the correlation between P9E2 and P12E2 is 0.72 with a gain of 2.1 dB.

## V. SUMMARY AND CONCLUSIONS

We presented the results of two separate measurement campaigns of the ultra wideband implant channel on living porcine subjects. A path loss model as a function of the propagation distance and frequency was developed for 5-16 cm and 1-6 GHz, respectively. To the best of our knowledge, this is the first ultra wideband in-body to on-body path loss model stemming from in-vivo measurements that has been reported in the literature. It is clear that the presented path loss model is antenna-dependent, and our future research will aim

This article has been accepted for publication in a future issue of this journal, but has not been fully edited. Content may change prior to final publication. Citation information: DOI 10.1109/JBHI.2015.2417805, IEEE Journal of Biomedical and Health Informatics

to improve the implantable antenna's radiating performance. This is a challenging problem, especially considering the limitations in size for real application in wireless implants. The use of several on-body receiving antennas to enhance the quality of the received signal was also investigated. The main conclusions that can be drawn from the presented results are:

1) Ultra wideband communications in low frequencies, i.e., 1-3 GHz, can reduce the transmission power consumption of wireless implants. Since the path loss is significantly lower in 1-3 GHz than in higher frequencies, regulations for the use of this band for ultra wideband implant communications should be pursued.

2) The use of multiple on-body receiving antennas is beneficial. It is plausible that power gains of 3 dB and above can be achieved if the antennas are place sufficiently close to each other.

3) There is a rather high correlation between different propagation paths, which may or may not be beneficial when constructing algorithms for signal processing and communications.

Another standing problem is the verification of the validity of our path loss model for humans. Although the anatomy of the porcine abdomen was deemed suitable by our medical advisors to approximate the human abdominal cavity, a thorough and fair comparison between numerical simulations with digital human body models and in-vivo measurements in swine has to be realized in the future. In order to achieve fairness, the same antenna types have to be used in both modeling approaches. Such a thorough validation lies beyond the scope of this paper. However, an initial comparison with the path loss model in [15] shows fair agreement between the simulation results therein and our in-vivo measurements. For instance, for a depth of 5 cm and a center frequency of 3.5 GHz, the simulation-based model estimates a path loss of 43 dB, whereas our so-called non-compensated model predicts 41 dB. For a depth of 10 cm and 3.5 GHz, the predicted path loss is 89 dB and 83 dB with the simulation-based and in-vivo non-compensated models, respectively. For the same depths and frequency, our compensated model predicts 39 dB and 81 dB, respectively. The agreement between these three different models demonstrates the usefulness of performing measurements in porcine subjects to characterize the path loss of ultra wideband signals propagating through the human body. Nevertheless, further research in this direction is required to firmly establish in-vivo measurements in swine as a standard radio propagation modeling technique for implants in humans.

## REFERENCES


[1] World Health Organization. *The global burden of chronic* [Online]. Available: http:// who.int/nutrition/topics/2_background/en/

[2] E. Y. Chow, M. M. Morris and P. Irazoqui, "Implantable RF medical devices," *IEEE Microwave*, vol. 14, no. 4, pp. 64-73, Jun. 2013.

[3] R. Hovorka, "Continuous glucose monitoring and closed-loop systems," *Diabetic Medicine*, vol. 23, no. 1, pp. 1-12, Jan. 2006.

[4] M. R. Yuce and T. Dissanayake, "Easy-to-swallow wireless telemetry," *IEEE Microwave*, vol. 13, no. 6, pp. 90-101, Sep./Oct. 2012.

[5] R. Chávez-Santiago, J. Wang and I. Balasingham, "The ultra wideband capsule endoscope," *IEEE Int. Conf. on Ultra-Wideband (ICUWB)*, Sydney, Australia, 2013, pp. 72-78.

[6] K. Thotahewa, J.-M. Redoute and M. R. Yuce, "A UWB wireless capsule endoscopy device," in *Proc. 36th Annual Int. Conf. of the IEEE Engineering in Medicine & Biology Society (EMBC)*, Chicago, IL, 2014, pp. 6977-6980.

[7] *IEEE Standard for Local and Metropolitan Area Networks–Part 15.6: Wireless Body Area Networks,* IEEE Standard 802.15.6-2012, 2012.

[8] R. Chávez-Santiago and I. Balasingham, "Ultrawideband signals in medicine [Life Sciences]," *IEEE Signal Process. Mag.*, vol. 31, no. 6, pp. 130-136, Nov. 2014.

[9] E. Zastrow, S. K. Davis and S. C. Hagness, "Safety assessment of breast cancer detection via ultrawideband microwave radar operating in pulsed-radiation mode," *Microwave and Optical Technology Letters*, vol. 49, no. 1, pp. 221-225, Jan. 2007.

[10] M. R. Yuce, H. C. Keong and M. Chae, "Wideband communication for implantable and wearable systems," *IEEE Trans. Microwave Theory Tech.*, vol. 57, no. 2, pp. 2597-2604, Oct. 2009.

[11] A. Khaleghi, R. Chávez-Santiago and I. Balasingham, "Ultra wideband pulse-based data communications for medical implants," *IET Communications*, vol. 4, no. 15, pp. 1189-1197, Oct. 2010.

[12] A. Daisuke, K. Katsu, R. Chávez-Santiago, Q. Wang, D. Plettemeier, J. Wang and I. Balasingham, "Experimental evaluation of implant UWB-IR transmission with living animal for body area networks," *IEEE Trans. Microw. Theory Techn.*, vol. 62, no. 1, pp. 183-192, Jan. 2014.

[13] J. Wang and Q. Wang, "Channel modeling and BER performance of an implant UWB body area link," in *Proc. 2nd Int. Symp. on Applied Sciences in Biomedical and Communication Technologies (ISABEL)*, Bratislava, Slovak Republic, 2009, pp. 1-4.

[14] A. Khaleghi, R. Chávez-Santiago and I. Balasingham, "Ultra-wideband statistical propagation channel model for implant sensors in the human chest," *IET Microwaves, Antennas & Propagation*, vol. 5, no.15, pp. 1805-1812, Dec. 2011.

[15] A. Khaleghi, R. Chávez-Santiago and I. Balasingham, "An improved ultra wideband channel model including the frequency-dependent attenuation for in-body communications," in *Proc. 34th Annual Int. Conf. of the IEEE Engineering in Medicine & Biology Society (EMBC)*, San Diego, CA, 2012, pp. 1631-1634.

[16] R. Chávez-Santiago, K. Sayrafian-Pour, A. Khaleghi, K. Takizawa, J. Wang, I. Balasingham and H.-B. Li, "Propagation models for IEEE 802.15.6 standardization of implant communication in body area networks," *IEEE Commun. Mag.*, vol. 51, no. 8, pp. 80-87, Aug. 2013.

[17] J. Shi, D. Anzai and J. Wang, "Channel modeling and performance analysis of diversity reception for implant UWB wireless link," *IEICE Trans. Commun.*, vol. E95-B, no. 10, pp. 3197-3205, Oct. 2012.

[18] M. M. Swindle, *Swine in the Laboratory: Surgery, Anesthesia, Imaging, and Experimental Techniques*. 2nd ed. Boca Raton, FL: CRC Press, 2007.

[19] Q. Wang, K. Wolf and D. Plettemeier, "An UWB capsule endoscope antenna design for biomedical communications," in *Proc. 3rd Int. Symp. on Applied Sciences in Biomedical and Communication Technologies (ISABEL)*, Rome, Italy, 2010, pp. 1-6.

[20] S. Brovoll, Ø. Aardal, Y. Paichard, T. Berger, T. R. Lande and S.-E. Hamran, "Optimal frequency range for medical radar measurements of human heartbeats using body-contact radar," in *Proc. 35th Annual Int. Conf. of the IEEE Engineering in Medicine & Biology Society (EMBC)*, Osaka, Japan, 2013, pp. 1752-1755.

[21] H. Yamamoto, J. Zhou and T. Kobayashi, **"**Ultra wideband electromagnetic phantoms for antennas and propagation studies**,"** *IEICE Transactions on Fundamentals of Electronics, Communications and Computer Sciences*, vol. E91-A, no. 11, pp. 3173-3182, Nov. 2008.

[22] *Channel Model for Body Area Network (BAN)*, IEEE P802.15-08-0780-12-0006, November 10, 2010.

[23] R. Chávez-Santiago and I. Balasingham, "Computation of the transmission frequency band for the ultra wideband capsule endoscope," in *Proc. 7th Int. Symp. on Medical Information and Communication Technology (ISMICT)*, Tokyo, Japan, 2013, pp. 66-70.

[24] T. Sereewattanapong and S. Promwong, "Evaluation of ultra wideband impulse radio transmission loss due to laptop computer," in *Proc. 9th Malaysia Int. Conf. on Communication*, Kuala Lumpur, Malaysia, 2009, pp. 259-262.

[25] S. Haykin, "*Communication Systems*," 3rd ed. John Wiley & Sons, Inc. 1994.

This article has been accepted for publication in a future issue of this journal, but has not been fully edited. Content may change prior to final publication. Citation information: DOI 10.1109/JBHI.2015.2417805, IEEE Journal of Biomedical and Health Informatics

**Pål Anders Floor** received his B.Sc. degree from Gjøvik University College (HIG), Gjøvik, Norway in 2001, his M.Sc degree in 2003 and his Ph,D, degree in 2008, both from the Department of Electronics and Telecommunications, Norwegian University of Science and Technology (NTNU), Trondheim, Norway. All three degrees are in electrical engineering.

He was working as a Post. Doc. at the Intervention Center at Oslo University Hospital as well as the Institute of Clinical Medicine at the University of Oslo from 2008-2013. He is currently a Post. Doc. at the Department of Electronics and Telecommunications at NTNU. His research include joint source-channel coding, information theory and signal processing applied on point-to-point links, in small and large networks, as well as in Neuroscience. He is currently doing research on communication issues for in-body sensors as well as lightweight cryptography for low complexity devices.

**Raúl Chávez-Santiago** was born in Oaxaca City, Mexico. He received the Ph.D. degree in electrical and computer engineering from Ben-Gurion University of the Negev, Israel, in 2007.

From 2007 to 2008 he held a Postdoctoral position at the University Paris-Sud XI, France, where he investigated radio resource management for mobile WiMAX systems. He later worked as a Postdoctoral Fellow at Bar-Ilan University, Israel, researching the information theory aspects of ad hoc and cognitive radio networking. He joined the Intervention Centre, Oslo University Hospital, Norway, in 2009, where he currently investigates short-range radio communication technologies for body area networks (BANs) and implantable biomedical sensor systems. He is a Management Committee member in various European COST Actions focusing in wireless communications, wireless power transmission, and biomedical topics.

**Sverre Brovoll** received the M.Sc. degree in cybernetics from the Norwegian University of Science and Technology, Trondheim, Norway, in 2006. In 2006, he started working with synthetic aperture radar systems as a scientist at the Norwegian Defence Research Establishment (FFI), Kjeller, Norway. In 2011, he began his work toward a Ph.D. degree in the field of medical radar systems at FFI and the department of informatics at the University of Oslo, Norway.

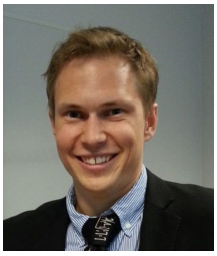

**Øyvind Aardal** received the M.Sc. degree in applied mathematics from the University of Oslo, Oslo, Norway, and the Ph.D. degree in 2008 and 2013, respectively.

In summer 2007, he was a Lecturer in mathematics at Oslo University College, Oslo, Norway. Since 2009, he has been with the Norwegian Defence Research Establishment (FFI), Kjeller, Norway, where he is currently working as a Scientist. His research interests include radar signal processing, target recognition and medical radar.

**Jacob Bergsland** biography was not available at time of publication.

**Ole-Johannes H. N. Grymyr** biography was not available at time of publication.

**Per Steinar Halvorsen** is a Chief Anesthesiologist at the Intervention Centre, Oslo University Hospital, Norway.

**Rafael Palomar** received the B.S. (2007) and M.S. (2010) degree in computer science from University of Córdoba, Spain. From 2010 to 2013, he has been a Software Engineer for The Intervention Centre at Oslo University Hospital, Norway, developing software for planning and navigation in image-guided surgery. He is currently working towards the Ph.D. degree at Gjøvik University College, Norway.

This article has been accepted for publication in a future issue of this journal, but has not been fully edited. Content may change prior to final publication. Citation information: DOI 10.1109/JBHI.2015.2417805, IEEE Journal of Biomedical and Health Informatics

**Dirk Plettemeier** received a diploma in Communication Engineering from the University of Applied Sciences in Lemgo and a diploma in Electrical Engineering from the University of Bochum, Germany. He received his Ph.D. degree from the University of Bochum in 2002.
He was employed at the Institute for High-Frequency Technique/Department of Antennas and Wave Propagation at University of Bochum until 2003. From 2003 until 2007 he was Head of the research group Numerical Calculation of High Frequency Electromagnetic Fields and Waves at the Electrotechnical Institute/Chair and Laboratory for Theory of Electromagnetic Fields and EMC at Technische Universität Dresden, Germany. From 2007 until 2010 he was head of the research group Antennas and Propagation at the Communication Laboratory. Since 2011, he holds the Chair for RF Engineering at Technische Universität Dresden.

**Svein-Erik Hamran** received an MSc in Technical Physics in 1984 from the Norwegian University of Science and Technology (NTNU, Trondheim, Norway) and a PhD degree in 1990 in Physics from the University of Tromsø, Norway.
He worked from 1985 to 1996 at the Environmental Surveillance Technology Programme and was in 1989/90 a Visiting Scientist at CNRS Service d'Aeronomie, Paris, France. From 1996 he has been at the Norwegian Defence Research Establishment working as a Chief Scientist managing radar programs. From 2001 to 2011 he was an Adjunct Professor in Near Surface Geophysics at the Department of Geosciences, University of Oslo. From 2011 he has been an Adjunct Professor at the Department of Informatics at the University of Oslo.
Prof. Hamran is the Principal Investigator of the Radar Imager for Mars' subsurFAce eXperiment – RIMFAX on the Mars 2020 NASA rover mission and a Co-Principal Investigator on the WISDOM GPR experiment on the ESA ExoMars rover. His main interest is UWB radar design, radar imaging and modelling in medical and ground penetrating radar.

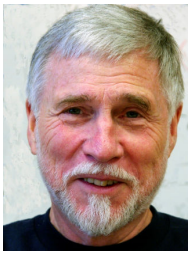

**Tor A. Ramstad** received his Siv.Ing. and Dr.Ing. degrees in 1968 and 1971, respectively, both from the Norwegian Institute of Technology (NTH) (now part of the Norwegian University of Science and Technology (NTNU)). He has held various positions at the Faculty of Electrical Engineering at the same university, and became a Full Professor of Telecommunications in 1983. From 2012, he is Professor Emeritus at NTNU. He has spent sabbaticals leaves at University of California, Santa Barbara (1982-83, 1997-98, 2008-09), at Georgia Institute of Technology (1989-90), and at EURECOM, France (2003-04, spring 2009). He was associate editor of IEEE Transactions on Acoustics, Speech, and Signal Processing, and a member of the IEEE DSP Technical Committee. He has chaired the Doctoral Committee NTH.
Dr. Ramstad is a member of the Norwegian Academy of Technical Sciences. His research interests are in the fields of multirate signal processing, speech and image processing with emphasis on compression, and joint source-channel coding.

**Ilangko Balasingham** received the M.Sc. and Ph.D. degrees from the Department of Electronics and Telecommunications, Norwegian University of Science and Technology (NTNU), Trondheim, Norway in 1993 and 1998, respectively, both in signal processing. He performed his Master's degree thesis at the Department of Electrical and Computer Engineering, University of California Santa Barbara, USA.
From 1998 to 2002, he worked as a Research Scientist developing image and video streaming solutions for mobile handheld devices at Fast Search & Transfer ASA, Oslo, Norway, which is now part of Microsoft Inc. Since 2002 he has been with the Intervention Centre, Oslo University Hospital, Norway, as a Senior Research Scientist, where he heads the Wireless Sensor Network Research Group. He was appointed Professor in Signal Processing in Medical Applications at NTNU in 2006. His research interests include super robust short-range communications for both in-body and on-body sensors, body area sensor network, microwave short range sensing of vital signs, short range localization and tracking mobile sensors, and nano-neural communication networks. He has authored or co-authored 190 journals and full conference papers, and has given 14 invited/ keynotes at international conferences.
In addition to organizing special sessions and workshops on wireless medical technology at the major conferences and symposiums, Prof. Balasingham served as General Chair of the 2012 Body Area Networks (BODYNETS) conference and serves as TPC Co-Chair of the 2015 ACM NANOCOM and Area Editor of Elsevier Nano Communication Networks. He is a Senior IEEE member.